Utilizing Spin-Down Transients for Vibration-Based Diagnostics of Resiliently Mounted Machines

Ryan Zachar, Peter Lindahl, John Donnal, William Cotta, Christopher Schantz, and Steven B. Leeb

***Abstract*— This paper presents a vibration measurement and analysis technique for use during a machine's spin-down procedure. During spin-down, the machine's operation covers a continuous wide frequency band, from operating speed to standstill, which allows the estimation of the machine's vibration transfer function (VTF). This transfer function is rich in information for detecting and differentiating not only machinery pathologies but also problems with vibrational mounts. Utilizing a back-electromotive force sensor to infer rotor speed and a single-axis accelerometer for vibration measurements, this technique allows minimally intrusive estimation of a machine's VTF. Data collected in laboratory and field tests aboard U.S. Navy ships are presented to demonstrate the usefulness of this monitoring technique.**

***Index Terms*— Condition monitoring, frequency response, generators, motors, rotating machines, transfer functions, vibration measurement, vibrations.**

I. Introduction

PROFILES for the maintenance of electromechanical systems arise from essentially three different engineering management strategies. Maintenance can occur when a system breaks or becomes excessively revealing, essentially deferring costs to a day of reckoning when the system is guaranteed to be unavailable. Alternatively, critical maintenance can occur on a scheduled or routine basis to attempt to ensure system availability though with recurring expenses. Or finally, one can attempt to optimize maintenance costs and system availability by working to predict needed repairs before systems become extreme failures [1]–[3]. This third option, often referred to as condition-based maintenance, is appealing in the sense that if the requisite condition monitoring is efficient and effective, a desired degree of mission capability can be achieved with well-reasoned expenses [1], [2].

For electromechanical systems, vibration measurements are often utilized as an input to condition-based maintenance decision making [1]–[4], and many organizations have issued standards for mechanical vibration and condition-based maintenance [5]–[7]. Further, researchers continue to develop condition monitoring and diagnostic procedures that utilize vibration sensors. For example, using various signal processing techniques, vibrational monitor outputs can be used to detect frequency modulations characteristic of ball bearing defects [8]–[11] and to supplement traditional motor current signature analysis in detecting rotor faults [12], [13].

The majority of these vibration-based algorithms rely on measurements taken at rated speeds. As such, the information gained for diagnostic purposes is limited to discrete excitation frequencies, i.e., the electrical and mechanical fundamental, harmonic, and modulated frequencies. This information, while clearly useful for specific diagnostic purposes, may lack the richness to distinguish actuator pathologies from a degraded mechanical structure, e.g., the vibration mounts. A machine's vibration transfer function (VTF), which relates excitation, e.g., rotor speed, to vibration over a range of operating speeds, offers a more complete view of the system and is commonly used to determine diagnostic information such as the natural resonance characteristics as well as noise transfer paths [14].

Empirical characterization of vibrational frequency responses in mechanical systems has traditionally required intrusive external excitation, e.g., a strike hammer or a shaker for wideband vibration analysis [14], [15]. Recently, nonintrusive methods have been developed, e.g., those that apply operational modal analysis (OMA) to ac machines for vibrational characterization [16]–[19]. However, as these methods rely on the response of the machinery system to small-magnitude random vibrational excitation, the intrinsic vibration caused by the machinery rotating during operation can make it difficult to determine the true vibrational modes of the system.

This paper presents an alternative nonintrusive approach for VTF characterization that takes advantage of a machine's spin-down. During turn OFF, a machine's operation covers a continuous wide frequency band, i.e., from rated operating speed to standstill. This operating interval of swept operation allows the estimation of the machine's VTF *in situ* and with minimal sensor installation. The advantage of this technique is that VTF characterization is made nonintrusively and from the intrinsic large-signal vibrational components as opposed to the small-magnitude random vibrational response used by OMA techniques. The remainder of this paper describes the minimal setup and the signal processing methods utilized for VTF extraction and demonstrates the spin-down estimation

Manuscript received November 4, 2015; revised January 28, 2016; accepted March 2, 2016. Date of publication March 31, 2016; date of current version July 7, 2016. The Associate Editor coordinating the review process was Dr. Ruqiang Yan.

R. Zachar is with the U.S. Navy, Bath, ME 04530 USA.

P. Lindahl is with the Research Laboratory of Electronics, Massachusetts Institute of Technology, Cambridge, MA 02139 USA (e-mail: lindahl@mit.edu).

J. Donnal is with the Massachusetts Institute of Technology, Cambridge, MA 02139 USA.

W. Cotta is with the U.S. Coast Guard, Washington, DC 20032 USA.

C. Schantz is with Infratek Solutions, Princeton Junction, NJ 08550 USA.

S. B. Leeb is with the Department of Mechanical Engineering, Massachusetts Institute of Technology, Cambridge, MA 02139 USA.

Color versions of one or more of the figures in this paper are available online at http://ieeexplore.ieee.org.

Digital Object Identifier 10.1109/TIM.2016.2540944

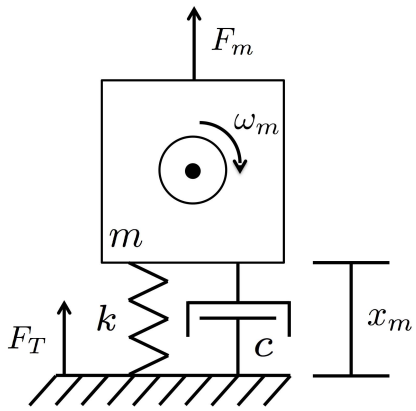

Fig. 1. 1-D free body diagram for the electromechanical machinery and mount system.

of the VTF in laboratory experiments and field applications aboard serving U.S. Navy warships.

II. Background

From a simplified perspective, an electric motor or generator mounted on resilient mounts can be modeled as a spring–mass–damper system with an eccentric mass vibration [15], as depicted in Fig. 1.

The equation that governs the motion of the actuator mass is

$$m\ddot{x}_m(t) + c\dot{x}_m(t) + kx_m(t) = F_m(t) \tag{1}$$

where m is mass, x_m is the position of the system, k is the spring constant, c is the damping ratio associated with the mount, t is time, and $F_m(t)$ is a forcing function. This equation can be rewritten in terms of system acceleration as

$$ma_m(t) + c\int_{-\infty}^{t} a_m(\tau)d\tau + k\iint_{-\infty}^{t} a_m(\tau)d\tau = F_m(t) \tag{2}$$

where $a_m(t)$ is the acceleration of the motor. Taking the Laplace transform of this equation and rearranging into transfer function form reveal the Laplace domain relationship between the acceleration $A_m(s)$ and the system forcing $F_m(s)$ as

$$\frac{A_m(s)}{F_m(s)} = \frac{\frac{s^2}{m}}{s^2 + \frac{c}{m}s + \frac{k}{m}} \tag{3}$$

where s is the Laplace transform operator.

For a rotating machine with an eccentric mass under steady-state conditions, this system forcing, $F_m(t)$, takes the form

$$F_m(t) = C\omega_m^2 \cos(\omega_m t) \tag{4}$$

where C is a constant related to load mass and imbalances and ω_m is the speed of the rotating shaft. A proportionally related virtual input function can be defined as

$$\Phi_m(t) = \omega_m^2 \cos(\omega_m t) \tag{5}$$

and its corresponding Laplace representation substituted into (3) to get

$$\frac{A_m(s)}{\Phi_m(s)} = \frac{C\frac{s^2}{m}}{s^2 + \frac{c}{m}s + \frac{k}{m}}. \tag{6}$$

This is the equation we refer to as the VTF in per kilogram assuming (5) maintains the units of (4).

Equation (5) is a function that can be derived from the motor speed ω_m. When combined with accelerometer measurements, this information can generate (6). This VTF is a transfer function that contains the same dynamic properties, e.g., natural frequency, as (3) and also scales as the forcing coefficient C changes, e.g., due to an increased load imbalance. During a motor spin-down when the speed is reducing from the motor's steady-state operating speed to standstill, speed and vibration sensors can be used to generate an empirical representation or empirical vibrational transfer function (eVTF) of (6) in that frequency range. The properties of this eVTF can then be used for machinery diagnostics.

Example Application: Machine Radiated Noise

One area of concern to many machinery operators is the force transmitted from the machine to the surface underneath F_T (Fig. 1). For example, a Navy ship may need to maintain its radiated acoustic noise at a minimum to avoid detection and an increase in force transmitted from the machine can lead to increased noise levels. With the knowledge of ω_n, an estimation of the force transmitted by the machine through its mounts to the supporting structure, relative to a value when the force is known to be acceptable, can be made from single accelerometer measurements on the machine system itself.

In steady state, an electromechanical machine has a transmissibility in the isolation range that is similar to that for zero damping. Therefore, c can be ignored as long as the operating speed is away from resonance [20], [21]. This means the force transmitted through the mounts to the base plate primarily occurs through the stiffness of the mounting (the spring in Fig. 1) and follows Hooke's law:

$$F_T \approx k \cdot x(t). \tag{7}$$

From (6), the natural frequency of this second-order system is given by $\omega_n = (k/m)^{1/2}$. Since the machine is following simple harmonic motion with acceleration described as $a(t) = A_{m,ss}\cos(\omega_{ss}t)$, where ss denotes steady-state conditions, (7) can be written in terms of m, ω_n, ω_{ss}, and $a(t)$ as:

$$F_T = -\frac{m\omega_n^2 a(t)}{\omega_{ss}^2}. \tag{8}$$

For diagnostic purposes, only the magnitude of F_T is of concern; taking the magnitude of (8) yields

$$|F_T| = \frac{m\omega_n^2 A_{m,ss}}{\omega_{ss}^2} \tag{9}$$

where A_m is the magnitude of the acceleration. In many situations, the system mass m and the machine's steady-state operating speed ω_{ss} are consistent whenever the machine is in normal operation. As such, an estimate of the ratio of force transmissions from a time when the machine is in a known good condition $|F_T|$ to the present condition $|F_T|'$ can be achieved from only acceleration and speed measurements of

the motor, that is

$$\frac{|F_T|'}{|F_T|} = \frac{\omega_n'^2 A'_{m,ss}}{\omega_n^2 A_{m,ss}}. \tag{10}$$

Here, ω_n^2 and $A_{m,ss}$ are parameters derived from spin-down measurements achieved with the machine in a known good condition, and $\omega_n'^2$ and $A'_{m,ss}$ are derived from the most recent measurements. Practically, (10) indicates the value of estimating the eVTF for (6) during machine spin-down. From the eVTF, it is possible to estimate the transfer function peak or, essentially, the natural frequency of the system from the observed resonant peak. Estimation of the natural frequency of the mount from the eVTF makes it possible to distinguish machine imbalance from degradation of the mount, both conditions that can cause increased transmitted vibration, which might be indistinguishable from steady-state measurements alone. Changes in the forcing function, e.g., the vibration energy created by operating the machine, will generally increase the magnitude of the entire eVTF. Aging or degradation of the mount alone will shift the resonant frequency of the eVTF. A comparison of successively observed eVTFs can be used to distinguish progressive imbalance from aging of the mount.

III. Sensor Measurements and eVTF Generation

In practice, estimation of the eVTF requires knowledge of the actuator vibration and speed during spin-down or during a similar operating sweep. We have developed an electronic sensor that can generate an eVTF without installation of a tachometer, strictly from relatively nonintrusive electrical measurements.

A. Data Collection

A single-axis accelerometer mounted vertically is used to measure vibration. This stream is considered the output of the system and requires little preprocessing other than scaling the output from millivolts to meters per second squared to provide the estimate, $\hat{A}_m(t)$.

The input to system (5) is estimated from the motor speed. This speed is inferred using a back electromotive force (back EMF) sensor measuring winding voltages on the machine. A back-EMF sensor is the preferred method for gathering spin-down speed as it is accurate, portable, and easy to install in the field. When a motor is disconnected from its power supply or the prime mover is turned OFF in the case of a generator, the rotor will continue spinning due to its inertia. Residual magnetism generates voltage on the stator. The characteristics of this voltage, e.g., amplitude and zero crossings, can then be used to estimate rotor speed.

The back EMF sensor (Fig. 2) employed in this paper uses noncontact differential capacitive sensing to detect the electric field generated by the phase lines of the machine. Three copper plates shown in Fig. 2(a) are secured against the insulating jackets of the phase lines inside the machine's terminal box. These plates are also electrically connected to a circuit with the simplified schematic shown in Fig. 2(b). Here, plate A (P_A) connects to the (+) side of the first

(a)

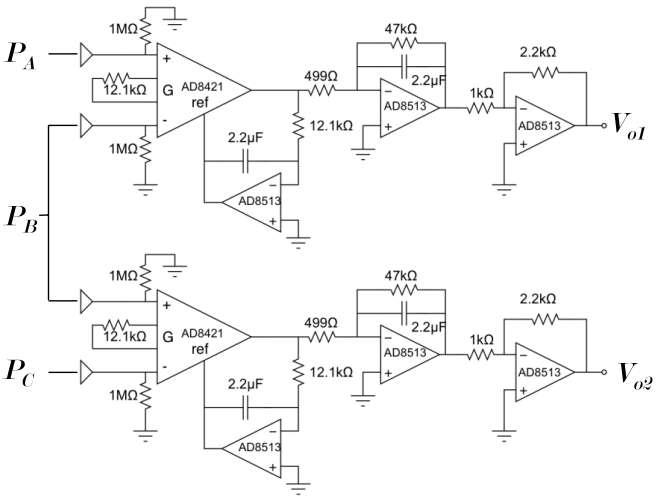

(b)

Fig. 2. Noncontact back-EMF sensor system used for estimating motor speed. (a) Photo of sensor plates. (b) Back EMF sensor schematic.

AD8421 differential amplifier, plate B (P_B) connects to the (−) side of the first AD8421 as well as the (+) side of the second AD8421, and plate C (P_C) connects to the (−) side of this second amplifier. These plates capacitively couple to the phase line voltages, V_A, V_B, and V_C, respectively. A more detailed explanation of the noncontact voltage sensor can be found in [22].

Under this configuration, the voltages generated at the outputs of the back EMF sensor are given by

$$V_{o1} = g_{a1}V_A - g_{b1}V_B + g_{n1}V_n \tag{11}$$

and

$$V_{o2} = g_{b2}V_B - g_{c2}V_C + g_{n2}V_n. \tag{12}$$

In these equations, V_n represents a common-mode background noise present at the output of the circuit and the g terms represent combined gains of the capacitive coupling and amplifier stages of the circuitry. The ratio $r_g = (g_{n1}/g_{n2})$ can be estimated by performing a scalar fit of $V_{o1} = r_g V_{o2}$ with measurements achieved when the machine is at standstill and

the phase voltages are zero. Then, the differential calculation, $V_o = V_{o1} - \hat{r}_g V_{o2}$, gives the voltage measurement

$$V_o = (g_{a1}V_A - g_{b1}V_B) - \hat{r}_g(g_{b2}V_B - g_{c2}V_C) \tag{13}$$

which has the common-mode noise term eliminated assuming the estimate $\hat{r}_g = r_g$. While this voltage signal does not have a physical meaning related to the system, it does preserve the mechanical speed to electrical speed and amplitude relationships.

This mechanical speed can be estimated from (13) in a number of ways based on the signal's amplitude and/or frequency. For this research project, if the following conditions are met, then the machinery spin-down speed profile is extracted from the signal envelope using a Hilbert transform based method.

1) There is no clipping in the back EMF sensor waveforms during steady-state operation.
2) There is no active electromagnetic control (e.g., braking) applied to the system during spin-down.

Here, the Hilbert transform produces a waveform linearly related to the signal amplitude. This waveform is then scaled to match the mechanical excitation speed ω_m based on the knowledge of the machine's steady-state speed rating. Further information on this method is given in [23] and [24].

If these conditions are not met, however, then the signal amplitude is not linearly related to speed throughout the entire spin-down. In this case, the electrical speed ω_e profile is achieved based on signal frequency estimates gained from a zero-crossing detection procedure. In this procedure, the k_{th} zero crossing is identified by a change of sign between two adjacent waveform samples at t_n and t_{n+1} and its time location $t[k]$ estimated based on the zero value of the linear interpolation of the signal values $V_o(t_n)$ and $V_o(t_{n+1})$. Then, the signal frequency at time instance $t[k]$ is estimated as

$$\hat{\omega}_e(t[k]) = \frac{2\pi}{t[k+1] - t[k-1]}. \tag{14}$$

In the above discussion, n represents the sample time index and k represents the time indexing of zero crossings.

In general, this method may be less noise immune than the Hilbert transform method as it is prone to uncertainty around zero crossings, particularly at low frequencies as the signal amplitude also decreases with speed. While many methods exist for accurate zero-crossing detection in noisy environments [25]–[27], for the purpose of gaining eVTF estimates here, all zero crossings including those generated by additive noise were detected as described above and outliers were removed prior to the frequency estimation of (14). From the $\hat{\omega}_e$ estimates, the mechanical speed estimate $\hat{\omega}_m$ is calculated based on the number of pole pairs in the machinery. Then, this stream is linearly interpolated to match the sampling rate of the original measurements for calculating the virtual input function $\Phi_m(t)$ from (5). Finally, the virtual input is calculated. In the case where the vibrational excitation is directly provided from eccentricities in the machine's rotor, $\Phi_m(t)$ is estimated from $\hat{\omega}_m(t)$ as

$$\Phi_m(t) = \hat{\omega}_m^2(t)\cos\left(\int_0^t \hat{\omega}_m(\tau)d\tau\right). \tag{15}$$

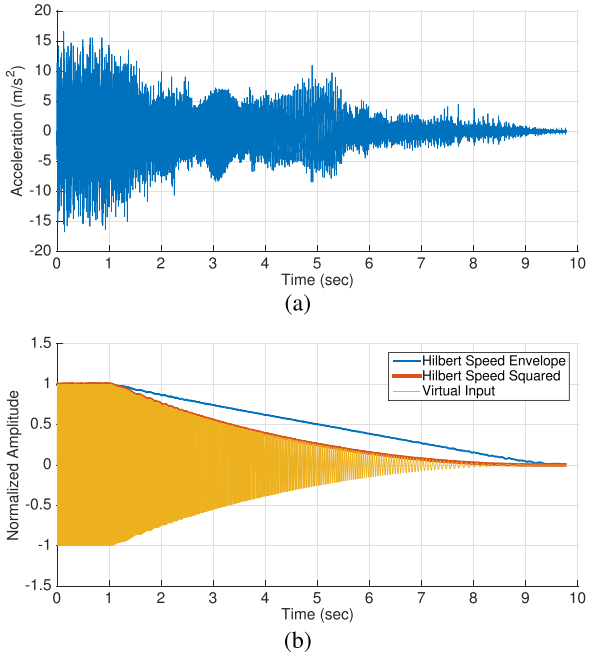

Fig. 3. Example time-domain signals used for eVTF generation. (a) Vibration sensor output. (b) Speed estimate and virtual input.

Examples of two time-domain signals required for the eVTF are shown in Fig. 3. Fig. 3 (top) shows the measured acceleration of the machinery during the spin-down, which starts around the 1-s mark, as noted by the beginning of the attenuation of the speed curves in Fig. 3 (bottom). Here, the curves are normalized by their peak values for simultaneous plotting. The blue curve shows the estimated speed, in this particular case, based on the Hilbert transform procedure. The orange curve shows the square of the blue curve and the yellow curve the calculated virtual input $\Phi_m(t)$.

B. Short-Time Fourier Transform Analysis

In accordance with (6), the time-domain spin-down signals of Fig. 3 need to be transformed into frequency domain signals. Empirically estimating a transfer function through spin-down analysis can be susceptible to noise from other nearby machinery [21]. Further complicating the process, the excitation frequency continuously changes with rotor speed. As such, the short-time Fourier transform (STFT) is used to process the signals to reduce uncorrelated noise and minimize frequency of excitation spreading in the analysis. Under this method, the time-domain waveforms are windowed at a series of time locations during the spin-down process and fast Fourier transform (FFT) is used to process each modified time signal resulting in a time-binned frequency representation of the original signals.

For this STFT application, a Hanning window is used as the mask for the input and output waveforms. This window is tunable through two parameters, the time width of the window T_w and the overlap between adjacent windows o_v. The Hanning windows are multiplied with the input and output waveforms to create masked versions. As an example, the windowing of the virtual input at the 1.5-s mark during a

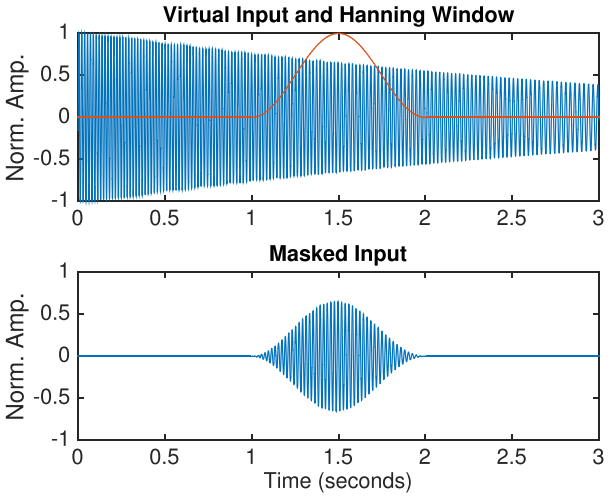

Fig. 4. Hanning window masking of the normalized virtual input centered at 1.5 s.

motor spin-down is shown in Fig. 4. The same process is also performed on the output.

The width parameter T_w represents a tradeoff between temporal resolution (improved by narrowing the window) and frequency resolution (improved by widening the window). In the context of this spin-down procedure, the rate at which the machine decelerates is the primary consideration for choosing T_w. If the spin-down is quick, a narrow window is required to have any time resolution. However, if the spin-down occurs slowly, then a wider window can be accommodated to improve the frequency resolution of the generated eVTF.

Similarly, the overlap parameter o_v represents a tradeoff between Hanning window boundary artifacts in the eVTF construction and the total computational energy required. That is, as the amount of overlap increases, the time gap between Hanning window centers decreases, thus reducing the artifacts of windowing the time-domain signal. However, this is at the expense of performing more Fourier transforms, which requires more computational energy.

A full series of Hanning-windowed inputs and outputs for a motor during spin-down is shown in Fig. 5. Here, the tunable parameters are set to $T_w = 1$ s and for clarity, $o_v = 0\%$. Fig. 5 (top, middle, and bottom) shows the individual windows and their time locations, the series of resulting masked virtual input waveforms, and the series of masked vibrational output waveforms, respectively.

Via the FFT, each Hanning-windowed input and output allows for the generation of a frequency spectrum specific to a short period of time during the spin-down process. These spectrums can be indexed as $\Phi_{m,i}(j\omega)$ and $A_{m,i}(j\omega)$, respectively, where i denotes the Hanning window index. A corresponding center frequency for each index can be defined as

$$\omega_i = \underset{\omega}{\operatorname{argmax}} \left| \frac{A_{m,i}(j\omega)}{\Phi_{m,i}(j\omega)} \right|. \tag{16}$$

To generate the eVTF, first all the output spectrums are

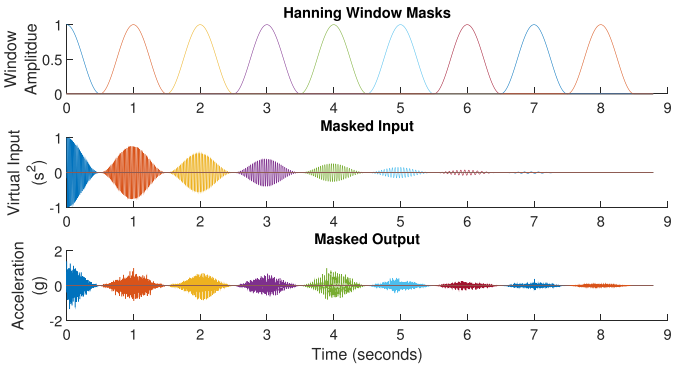

Fig. 5. Hanning windows and masked inputs and outputs.

masked around the corresponding center frequencies such that

$$A'_{m,i}(j\omega) = \begin{cases} 0 & \omega \le \omega_i - w/2 \\ A_{m,i}(j\omega) & \omega_i - w/2 \le \omega \le \omega_i + w/2 \\ 0 & \omega \ge \omega_i + w/2 \end{cases} \tag{17}$$

where the variable w limits the valid vibrational response frequencies to those around the frequency of virtual input excitation. This is done to preserve linearity in the eVTF and to ignore sources of noise at extraneous frequencies. Maximum envelope excitation and response spectrums are then defined as

$$\Phi_{\text{env}}(j\omega) = \max_i \left[\underset{\Phi_{m,i}(j\omega)}{\operatorname{argmax}} |\Phi_{m,i}(j\omega)| \right] \tag{18}$$

and

$$A_{\text{env}}(j\omega) = \max_i \left[\underset{A'_{m,i}(j\omega)}{\operatorname{argmax}} |A'_{m,i}(j\omega)| \right] \tag{19}$$

respectively. That is, at a given frequency, these envelopes are defined as equal to the corresponding indexed spectrum with the maximum magnitude at that particular frequency. The eVTF is then determined as

$$\frac{A_m(j\omega)}{\Phi_m(j\omega)} = \frac{A_{\text{env}}(j\omega)}{\Phi_{\text{env}}(j\omega)}. \tag{20}$$

Generating the eVTF in this manner allows the maximum amount of information gained during the STFT-based analysis to be passed on to the eVTF while also ensuring linearity.

Fig. 6 shows a graphical representation of this process. In Fig. 6, the magnitudes shown on the y-axis are normalized to the maximum values of each input and output spectrum series, $\Phi_{m,i}(j\omega)$ and $A_{m,i}(j\omega)$, respectively. The dashed curves represent the STFT envelopes of (18) and (19), while the solid lines represent individual spectrums from a windowed time segment roughly half-way through the spin-down. This particular period also corresponds to the peak resonance in the system. Fig. 6 shows that the FFT for the virtual input signal has a maximum at around 31.5 Hz, while the resulting FFT for the output vibration signal has a maximum at around 33 Hz. This offset is due to the fact that there is a time delay in the vibrational response to the forcing input. For this analysis, the width parameter w for the output response is set to 6 Hz. As such, the indexed response spectrum is cut off at the frequencies of 28.5 and 34.5 Hz to ensure that the maximum

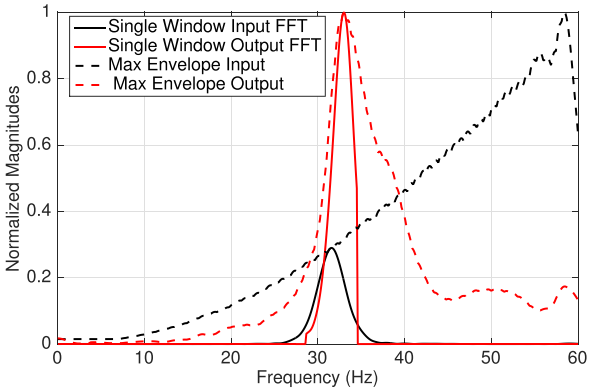

Fig. 6. Fast Fourier transform of masked inputs and masked outputs with envelopes.

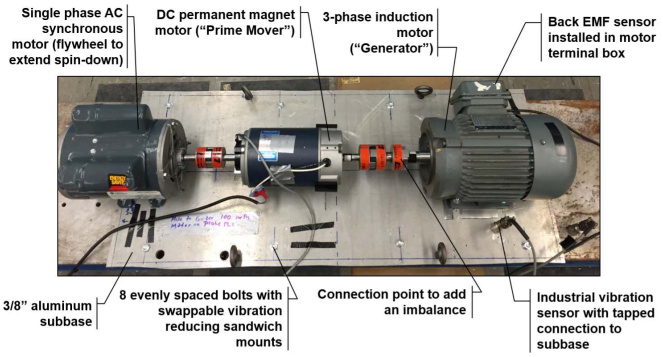

Fig. 7. Image showing the purpose-built machine set for testing eVFT generation and machinery trends useful in diagnostics.

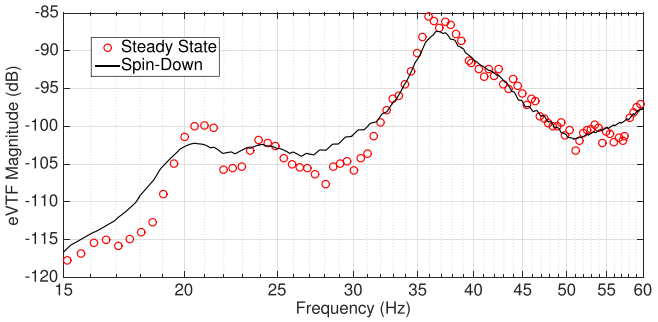

Fig. 8. Comparison of a spin-down derived eVTF and steady-state measurement derived eVTF.

envelope is created from the linear vibrational response, while still allowing the capturing of the delayed peak response. This particular analysis results in the eVTF plot for the 50-A durometer mounts in Fig. 9.

IV. Tests on Purpose-Built Machine Set

To test the method for generating the eVTFs as described in the previous section and to showcase the application of this hardware and signal processing for machinery diagnostics, a test stand consisting of a prime mover, inertia load, and a generator was constructed. This test stand, shown in Fig. 7, centers around a dc permanent magnet motor with dual couplings. One end is coupled to a three-phase induction machine and the other is connected to a single-phase synchronous ac motor, which is disabled and acts only as a flywheel. The three machines are mounted onto a single metal sub-base, as is typical for many industrial actuator installations. The sub-base is mounted to a steel box girder with vibration reducing mounts at eight points. A second shaft coupler is attached to the induction motor as an attachment point for an imbalance. This is done to simulate a rotor imbalance, a type of machinery fault, which should appear in the eVTF as an increase in vibration magnitude at resonance. Five commercial vibration dampening mounts of different durometers (30, 40, 50, 60, and 70 A) were used to emulate a scenario where the mounts' stiffness increases or decreases over time, the effect of which should appear in the eVTF as a shift in resonance.

A. Comparison of Spin-Down eVTF and Steady-State eVTF

Initial tests were performed on a subset of mounts to validate the eVTFs generated during the machinery spin-down by comparing them with eVTFs generated from steady-state measurements. A Python script is used to automate the steady-state measurement collection by commanding a series of dc voltages from a power supply connected to the dc motor. At each discrete voltage level, the script reads motor speed from a shaft encoder and measures the sub-base vibration with a standard industrial accelerometer. The script removes data collected prior to when the machines reach steady state at each voltage level and the remaining vibration data are analyzed using Welch's power spectral density estimate [28]. At each voltage level, the peak of the power spectral density at a frequency closest to but greater than the measured speed of the motor is taken as the vibration magnitude at the measured speed. Finally, each corresponding measured operating speed is squared to generate a virtual input for generation of the steady-state eVTF.

Fig. 8 gives a comparison of a spin-down eVTF with a steady-state eVTF for the 60-A durometer mounts and machine setup described above. For this particular test, the dc motor was run in steady state at 105 discrete voltage levels with 4 s of steady-state operation at each resulting motor speed. The spin-down eVTF was calculated from the data collected following the motor's power supply turning OFF after the maximum voltage level was reached. This spin-down process took approximately 10 s and the analysis parameters were set to $T_w = 1$ s, $o_v = 90\%$, and $w = 3$ Hz.

As seen in Fig. 8, the two curves are very similar and show the same resonant peak, indicating that the spin-down procedure accurately captures the important features of the system's VTF. The spin-down eVTF appears much smoother with less variance in measurements because the virtual input is derived from the Hilbert Transform and low-pass filtered rather than calculated directly from speed measurements, as is the case for the steady-state eVTF. This particular result is well representative of the results gained from other durometer mounts.

It should be noted that the number of features present in the eVTFs exceeds those allowed by the second-order model

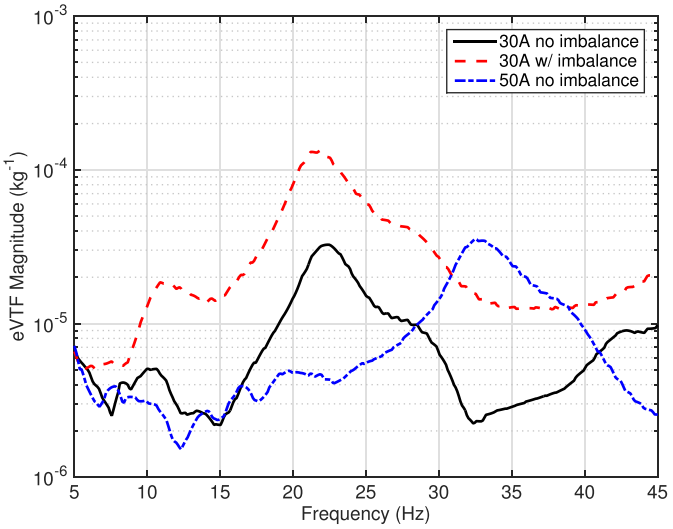

Fig. 9. eVTFs from the tests of the 30- and 50-A mounts showing a shift in natural frequency with a change in durometer and an increase in amplitude due to an increase in system imbalance.

TABLE I
COMPARISON OF eVFT CHARACTERISTICS FOR VARIOUS DUROMETER MOUNTS AND ROTOR IMBALANCES

Durometer	Imbalance (g)	Number of Tests	Natural Frequency (Hz) [mean (*std*)]	Peak Amplitude (kg^{-1}) [mean (*std*)]
30A	0	4	22.3 (*0.170*)	32.5 (*1.98*) $\times 10^{-6}$
	17	4	21.8 (*0.153*)	136 (*1.45*) $\times 10^{-6}$
40A	0	4	26.1 (*0.117*)	39.9 (*0.463*) $\times 10^{-6}$
	17	4	25.6 (*0.125*)	158 (*1.38*) $\times 10^{-6}$
50A	0	4	32.7 (*0.193*)	36.1 (*0.386*) $\times 10^{-6}$
	17	2	31.2 (*0.155*)	143 (*2.20*) $\times 10^{-6}$
60A	0	4	38.5 (*0.108*)	33.2 (*0.387*) $\times 10^{-6}$
	17	3	36.4 (*0.122*)	134 (*10.55*) $\times 10^{-6}$
70A	0	5	44.3 (*0.195*)	41.2 (*0.887*) $\times 10^{-6}$
	17	4	41.4 (*0.083*)	161 (*1.92*) $\times 10^{-6}$

described in Section II. This is due to the fact that the model assumes a single degree of freedom (DOF) and linearity in the system, while real-world machinery systems have 3 DOF and many sources of nonlinearity. Nevertheless, for the purposes of diagnostics, e.g., sensing changes in transferrable noise, the measured eVTF around the resonant peak approximates a second-order system and provides useful parametric estimations, as illustrated in the following.

B. eVTFs With Condition Changes

With confidence in the eVTF method described, the process was applied to a total of ten conditions across the five mount types and with and without a 17-g imbalance attached to the rotor system. These tests were done to show the utility of the eVTF method toward machinery diagnostics in accordance with the example application described in Section II. The premise of this method is that eVTFs gained opportunistically during a machinery spin-down can provide useful information, e.g., changes in vibration amplitude and resonant frequency, indicative of system failures, i.e., machinery imbalance and mount degradation, respectively.

Fig. 9 illustrates this premise with eVTFs gained during testing. In Fig. 9, the solid black curve shows the eVTF gained during machinery spin-down when 30-A mounts were installed and no additional imbalance was applied to the system. This curve shows a resonant peak just above 22 Hz at a magnitude of approximately 3.2×10^{-5} kg^{-1}. When the 17-g imbalance was added to the shaft, the magnitude of the vibration increased significantly, but without a significant shift in resonance as shown by the dashed red plot, which has a peak around 1.4×10^{-4} kg^{-1} at just under 22 Hz. However, when 50-A durometer mounts were used without an imbalance, while the magnitude of the eVTF remained similar (approximately 3.6×10^{-5} kg^{-1}), the resonant frequency shifted significantly to 33 Hz (dashed–dotted blue curve). Thus, the spin-down generated eVTF increases the amount of distinguishing information available to an operator in diagnosing issues in the machinery system.

Table I compiles the results from all tests involving the five mount types described above. The third column of Table I indicates the total number of tests performed on each mount and imbalance. Mean values from each set of tests for the system's natural frequency and peak eVTF amplitude are given in columns four and five, respectively. In addition, in each of these columns, the accompanying standard deviations are included to give an indication of repeatability. As observed there, the tests are very consistent for each configuration with the standard deviation in measured natural frequency less than 1% of the mean value and that of the peak amplitude less than 8% for all tests.

Example Fault Detection: When considering steady-state acceleration measurements, the usefulness of the eVTF results of Fig. 9 and Table I becomes clear. For the three cases shown in Fig. 9, the 30-A durometer mounts with no imbalance, the 30-A durometer mounts with imbalance, and the 50-A durometer mounts with no imbalance had steady-state rms accelerometer measurements of 0.031, 0.072, and 0.028 m/s^2, respectively. In these tests, the 30-A durometer test with no imbalance represents the system's baseline performance, while the other two tests represent that under two fault types, rotor imbalance, and mount stiffening.

If the headroom for allowable transmitted vibration is double that of the baseline result, then only the steady-state accelerometer measurements when the rotor is imbalanced would indicate a potential fault as it increased by a factor of 2.3 over the baseline case. When the 50-A mounts were installed to simulate mount stiffening, the steady-state accelerometer measurement actually slightly decreased by 10%. However, from the eVTF results, information on the natural frequency is also available. Using (10), the change in the transmitted vibration is then actually predicted as double that of the baseline result and indicative of a fault because the system's natural frequency shifted from 22.3 to 32.7 Hz (see Table I).

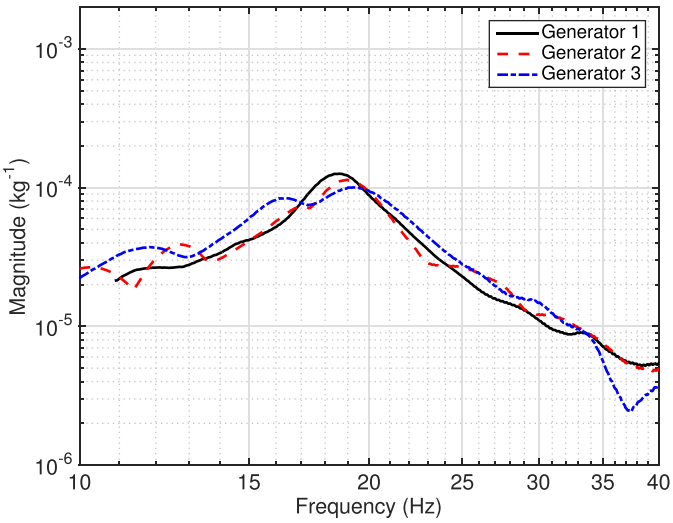

Fig. 10. MCM generator eVTFs as measured during generator spin-downs.

V. Field Tests on U.S. Navy Equipment

A series of field tests were conducted on an active U.S. Navy mine countermeasures ship (MCM). The ship has three ship service diesel generators (SSDGs) each rated at 375 kW. Each generator set is mounted on a metal sub-base, which is attached to the hull of the ship via eight resilient mounts in a configuration similar to the laboratory setup described in the previous section. The U.S. Navy is interested in nonintrusive, *in situ* characterization of these mounts for tracking changes in the vibration energy passed to the hull of the ship. The work described here is part of a larger project to integrate a self-sustaining sensor [24], [29], [30] inside the SSDG terminal box, which would alert the operator when the mounts are beginning to degrade. For this experiment, however, the standard industrial accelerometers and the back EMF sensors described earlier were used.

Each generator set contains a six-cylinder four-stroke diesel engine for driving the prime mover at 30 Hz (1800 r/min). As such, the vibration measurements contain a fundamental spin-down component that starts in the steady-state at 30 Hz. However, during all generator tests, a stronger vibrational component was observed with a 45-Hz fundamental in the steady state. This off-harmonic content is likely caused by imbalances in fuel mixture distribution and uneven piston firing in the diesel engine [31], [32]. For the subsequent analysis presented here, this stronger vibrational component was used to generate the eVTF plots, with the virtual input appropriately scaled so that

$$\Phi_m(t) = (1.5\hat{\omega}_m(t))^2 \cos\left(1.5\int_0^t \hat{\omega}_m(\tau)d\tau\right). \qquad (21)$$

In addition, during these tests, the back EMF sensor outputs were observed to be clipping in the steady state, so the zero-crossing method was used for estimating ω_m. The spin-down of these generators took approximately 25 s and the analysis parameters were set to $T_w = 1$ s, $o_v = 90\%$, and $w = 4$ Hz.

A total of 14 spin-downs were measured on the generators under various ship conditions, including while the ship was in port with no other machinery operating and underway when several other pieces of machinery were simultaneously operating. Fig. 10 shows example eVTFs gained during spin-down of each of the three ship generators, and Table II compiles the statistical characteristics for all the eVTFs tests performed. Fig. 10 shows clear resonant peaks in all three generators around 19 Hz and all with a similar amplitude of approximately 10^{-4} kg^{-1}. These curves are well representative of all the eVTFs gained for each corresponding generator, regardless of the ship's condition, and simultaneous electro-mechanical load use. This is confirmed by comparing the standard deviations in resonant peak amplitude and frequency locations with their corresponding mean values in Table II. Here, for all tests, the standard deviation in peak amplitude estimates was less than 8% of the mean, while those in the peak amplitude frequency locations were less than 1% for each test. Thus, while there is little exposed by these tests to differentiate any physical characteristics of each generator, the consistency in each test gives confidence in the repeatability of the method. Additional research is required to track the evolution of the eVTF characteristics over a longer period of time, and plans are in place to do so as a part of future self-sustained sensor developments discussed in [24], [29], and [30].

In addition to the generator experiments, vibrational analysis tests were performed on two of the ship's auxiliary seawater (ASW) pumps. Each pump operates at 59 Hz (3545 r/min) and is driven by a three-phase induction motor rated at 15 kW (20 hp). The crew had noted that one of the ASW pumps (Pump 2) had recently been overhauled, while

TABLE II
Statistical Characteristics for the eVTFs Gained During MCM Generator Spin-Down

Generator Number	Number of Tests	Natural Frequency (Hz) [mean (*std*)]	Peak Amplitude (kg^{-1}) [mean (*std*)]
1	5	18.4 (*0.146*)	136 (*9.12*) $\times 10^{-6}$
2	5	19.0 (*0.109*)	103 (*7.77*) $\times 10^{-6}$
3	4	19.2 (*0.0618*)	96.8 (*4.35*) $\times 10^{-6}$

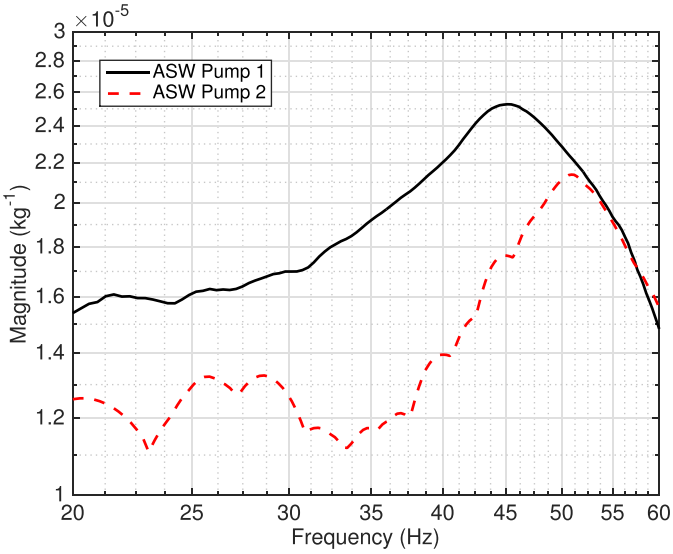

Fig. 11. ASW pumps 1 and 2 spin-down generated eVTFs.

TABLE III
STATISTICAL CHARACTERISTICS FOR THE eVTFs GAINED DURING AUXILIARY SEAWATER PUMP SPIN-DOWNS

Pump Number	Number of Tests	Natural Frequency (Hz) [mean (*std*)]	Peak Amplitude (kg^{-1}) [mean (*std*)]
1	8	44.7 (*0.328*)	26.0 (*0.359*) $\times 10^{-6}$
2	8	50.9 (*0.629*)	20.4 (*0.750*) $\times 10^{-6}$

the overhaul date of the other pump (Pump 1) was unknown. The spin-down times for these pumps were approximately 4 s. As such, the window-width parameter T_w was shortened to 0.25 s, the overlap parameter o_v was increased to 95%, and the masking width w set to 8 Hz. Example eVTFs resulting from this analysis are shown in Fig. 11, while Table III give the statistical characteristics of all tests performed.

As can be seen in Fig. 11, there are characteristic differences between the two pump eVTFs with the recently overhauled ASW Pump 2 showing a peak magnitude about 14% lower than ASW Pump 1 and at a frequency about 6 Hz higher. The results shown here are well representative of all the tests performed on the two pumps, as observed in Table III, which shows that the standard deviation in the resonant peak amplitude was less than 4% of the mean and that of its frequency location less than 1.5% of the mean for both pumps.

While Fig. 11 shows more compelling differences between machines than the eVTFs generated from the generator spin-downs (Fig. 10), concrete conclusions on the causes of these differences cannot be made. The most recently overhauled pump (ASW 2) does show a decreased magnitude in its eVTFs compared with those of ASW 1, though their resonant peak frequency locations are increased, which as shown in Section IV, would suggest a stiffening of the rubber typical of aging mounts. Still, these characteristic differences were clear and repeatable for all tests.

VI. CONCLUSION

This paper demonstrates the usefulness of a nonintrusive vibration measurement and analysis technique for use during an electromechanical machine's spin-down procedure. As the speed of the machine decreases from its normal operating speed to standstill, the process inherently provides vibrational excitation swept across a range of frequencies, permitting the estimation of the VTF (eVTF). As shown in laboratory tests, this transfer function reveals characteristics useful for machinery diagnostics, which are unavailable for estimation during steady-state operation. The consistency of the field test results combined with the interpretability of laboratory test results demonstrates that this analysis method can provide useful information for electromechanical machinery diagnostics.

Concretely, observing the eVTF is useful for disaggregating faults caused by changes in the machinery, e.g., an imbalance increasing the magnitude of the eVTF profile, from faults caused by the mounts, e.g., mount stiffening increasing the natural frequency of the eVTF profile. It is also useful for estimating changes in the extent of vibrational noise transmitted through the resilient mounts at steady state, as described in (10). Thus, through this technique, a user can estimate the significance of increased vibration on transmitted noise. Then, if the source is determined to be mechanical, the user can utilize previously established methods for delineating sources of mechanical vibration [2]–[4], [8]–[11].

This eVTF approach with back EMF sensing is intended to be deployed as part of a self-contained sensor [24], [29], [30], which can be installed within the terminal box of a machine. However, the technique can easily use any speed sensor with adequate resolution and sample rate for varying capabilities, e.g., using an optical sensor for improved portability. In either case, the method provides effective and useful information about both electromechanical machinery and the health of an associated mount.

ACKNOWLEDGMENT

The authors would like to thank the Office of Naval Research Structural Acoustics Program and the Grainger Foundation.

REFERENCES

[1] S. K. Yang, "A condition-based failure-prediction and processing-scheme for preventive maintenance," *IEEE Trans. Rel.*, vol. 52, no. 3, pp. 373–383, Sep. 2003.
[2] A. K. S. Jardine, D. Lin, and D. Banjevic, "A review on machinery diagnostics and prognostics implementing condition-based maintenance," *Mech. Syst. Signal Process.*, vol. 20, no. 7, pp. 1483–1510, 2006.
[3] A. Heng, S. Zhang, A. C. C. Tan, and J. Mathew, "Rotating machinery prognostics: State of the art, challenges and opportunities," *Mech. Syst. Signal Process.*, vol. 23, no. 3, pp. 724–739, 2009.
[4] S. Nandi, H. A. Toliyat, and X. Li, "Condition monitoring and fault diagnosis of electrical motors—A review," *IEEE Trans. Energy Convers.*, vol. 20, no. 4, pp. 719–729, Dec. 2005.
[5] *Condition Monitoring and Diagnostics of Machines—Requirements for Qualifiication and Assessment of Personnel—Part 2: Vibration Condition Monitoring and Diagnostics*, document ISO 18436-2:2014, International Organization for Standardization, May 2014.
[6] NAVSEA, "Department of defense test method standard: Mechanical vibrations of shipboard equipment (type I—Environmental and type II—Internally excited)," U.S. Dept. Defense, Tech. Rep. MIL-STD-167-1A, 2005.
[7] NAVSEA, "Structure-borne vibratory acceleration measurements and acceptance criteria of shipboard equipment," U.S. Dept. Defense, Tech. Rep. MIL-STD-740/2, 1986.
[8] J. R. Stack, R. G. Harley, and T. G. Habetler, "An amplitude modulation detector for fault diagnosis in rolling element bearings," *IEEE Trans. Ind. Electron.*, vol. 51, no. 5, pp. 1097–1102, Oct. 2004.
[9] C. Bianchini, F. Immovilli, M. Cocconcelli, R. Rubini, and A. Bellini, "Fault detection of linear bearings in brushless AC linear motors by vibration analysis," *IEEE Trans. Ind. Electron.*, vol. 58, no. 5, pp. 1684–1694, May 2011.
[10] I. Bediaga, X. Mendizabal, A. Arnaiz, and J. Munoa, "Ball bearing damage detection using traditional signal processing algorithms," *IEEE Instrum. Meas. Mag.*, vol. 16, no. 2, pp. 20–25, Apr. 2013.
[11] A. Soualhi, K. Medjaher, and N. Zerhouni, "Bearing health monitoring based on Hilbert–Huang transform, support vector machine, and regression," *IEEE Trans. Instrum. Meas.*, vol. 64, no. 1, pp. 52–62, Jan. 2015.
[12] C. Concari, G. Franceschini, and C. Tassoni, "Differential diagnosis based on multivariable monitoring to assess induction machine rotor conditions," *IEEE Trans. Ind. Electron.*, vol. 55, no. 12, pp. 4156–4166, Dec. 2008.
[13] V. Climente-Alarcon, J. A. Antonino-Daviu, F. Vedreno-Santos, and R. Puche-Panadero, "Vibration transient detection of broken rotor bars by PSH sidebands," *IEEE Trans. Ind. Appl.*, vol. 49, no. 6, pp. 2576–2582, Nov./Dec. 2013.
[14] A. Brandt, *Noise and Vibration Analysis: Signal Analysis and Experimental Procedures*. New York, NY, USA: Wiley, 2011.
[15] Z. Tang, P. Pillay, and A. M. Omekanda, "Vibration prediction in switched reluctance motors with transfer function identification from shaker and force hammer tests," *IEEE Trans. Ind. Appl.*, vol. 39, no. 4, pp. 978–985, Jul./Aug. 2003.

[16] R. Pintelon, B. Peeters, and P. Guillaume, "Continuous-time operational modal analysis in the presence of harmonic disturbances," *Mech. Syst. Signal Process.*, vol. 22, no. 5, pp. 1017–1035, 2008. [Online]. Available: http://www.sciencedirect.com/science/article/pii/S0888327007002592
[17] P. Mohanty and D. J. Rixen, "Operational modal analysis in the presence of harmonic excitation," *J. Sound Vibrat.*, vol. 270, nos. 1–2, pp. 93–109, 2004. [Online]. Available: http://www.sciencedirect.com/science/article/pii/S0022460X03004851
[18] P. Mohanty and D. J. Rixen, "Identifying mode shapes and modal frequencies by operational modal analysis in the presence of harmonic excitation," *Experim. Mech.*, vol. 45, no. 3, pp. 213–220, 2005.
[19] A. Agneni, G. Coppotelli, and C. Grappasonni, "A method for the harmonic removal in operational modal analysis of rotating blades," *Mech. Syst. Signal Process.*, vol. 27, pp. 604–618, Feb. 2012. [Online]. Available: http://www.sciencedirect.com/science/article/pii/S0888327011003815
[20] L. L. Beranek and I. L. Vér, Eds., *Noise and Vibration Control Engineering: Principles and Applications*. New York, NY, USA: Wiley, 1992.
[21] C. J. Schantz, "Methods for non-intrusive sensing and system monitoring," Ph.D. dissertation, Dept. Mech. Eng., Massachusetts Inst. Technol., Cambridge, MA, USA, 2014.
[22] J. S. Donnal and S. B. Leeb, "Noncontact power meter," *IEEE Sensors J.*, vol. 15, no. 2, pp. 1161–1169, Feb. 2015.
[23] J. O. Smith, *Mathematics of the Discrete Fourier Transform (DFT)*, 2nd ed. W3K Publishing, 2007. [Online]. Available: http://www.w3k.org/books/
[24] J. S. Donnal *et al.*, "VAMPIRE: Accessing a life-blood of information for maintenance and damage assessment," in *Proc. Amer. Soc. Naval Eng.*, 2012, pp. 132–142.
[25] D. Grillo, N. Pasquino, L. Angrisani, and R. Schiano Lo Moriello, "An efficient extension of the zero-crossing technique to measure frequency of noisy signals," in *Proc. IEEE Int. Instrum. Meas. Technol. Conf. (I2MTC)*, May 2012, pp. 2706–2709, doi: 10.1109/I2MTC.2012.6229703.
[26] R. W. Wall, "Simple methods for detecting zero crossing," in *Proc. 29th Annu. Conf. IEEE Ind. Electron. Soc. (IECON)*, vol. 3. Nov. 2003, pp. 2477–2481.
[27] O. Vainio and S. J. Ovaska, "Digital filtering for robust 50/60 Hz zero-crossing detectors," *IEEE Trans. Instrum. Meas.*, vol. 45, no. 2, pp. 426–430, Apr. 1996.
[28] P. D. Welch, "The use of fast Fourier transform for the estimation of power spectra: A method based on time averaging over short, modified periodograms," *IEEE Trans. Audio Electroacoust.*, vol. AU-15, no. 2, pp. 70–73, Jun. 1967.
[29] J. Moon, J. Donnal, J. Paris, and S. B. Leeb, "VAMPIRE: A magnetically self-powered sensor node capable of wireless transmission," in *Proc. 28th Annu. IEEE Appl. Power Electron. Conf. Expo. (APEC)*, Mar. 2013, pp. 3151–3159.
[30] J. Moon and S. B. Leeb, "Analysis model for magnetic energy harvesters," *IEEE Trans. Power Electron.*, vol. 30, no. 8, pp. 4302–4311, Aug. 2015.
[31] K. J. Sigmund, S. J. Shelley, M. Bauer, and F. Heitkamp, "Analysis of vehicle vibration sources for automatic differentiation between gas and diesel piston engines," *Proc. SPIE*, vol. 8391, pp. 839109-1–839109-15, May 2012.
[32] M. Bodden and R. Heinrichs, "Diesel sound quality analysis and evaluation," in *Proc. Forum Acusticum*, 2005, pp. 1–4.

Ryan Zachar received the M.S. degree from the Massachusetts Institute of Technology, Cambridge, MA, USA, in 2015.

He currently serves as an Officer of the U.S. Navy, Philadelphia, PA, USA.

Peter Lindahl received the Ph.D. degree in engineering from Montana State University, Bozeman, MT, USA, in 2013.

He is currently a Post-Doctoral Associate with the Research Laboratory of Electronics, Massachusetts Institute of Technology, Cambridge, MA, USA. His current research interests include sensors and instrumentation for energy and power systems, renewable energy generation, and energy policy.

John Donnal received the B.S. degree in electrical engineering from Princeton University, Princeton, NJ, USA, in 2007, and the M.S. degree in electrical engineering from the Massachusetts Institute of Technology, Cambridge, MA, USA, in 2013, where he is currently pursuing the Ph.D. degree.

His current research interests include nonintrusive load monitoring synthesis, energy harvesting, and communications systems.

William Cotta received the M.S. degree in mechanical engineering from the Massachusetts Institute of Technology, Cambridge, MA, USA, in 2015.

He currently serves as an Officer of the U.S. Coast Guard, Washington, DC, USA.

Christopher Schantz received the B.S. degree from the California Institute of Technology, Pasadena, CA, USA, in 2008, and the M.S. and Ph.D. degrees from the Massachusetts Institute of Technology, Cambridge, MA, USA, in 2011 and 2014, respectively, all in mechanical engineering.

He is currently the Chief Technology Officer with Infratek Solutions, Princeton, NJ, USA (Infratek Solutions is not affiliated with this research). His current research interests include signal processing for sensing and control systems.

Steven B. Leeb received the Ph.D. degree from the Massachusetts Institute of Technology (MIT), Cambridge, MA, USA, in 1993.

He has been a Faculty Member with the Department of Electrical Engineering and Computer Science, MIT, since 1993, where he currently holds a joint appointment with the Department of Mechanical Engineering. His current research interests include the development of signal processing algorithms for energy and real-time control applications.